DANISH METEOROLOGICAL INSTITUTE

SCIENTIFIC REPORT

01-02

Radioholographic methods for processing radio occultation data in multipath regions

M. E. Gorbunov

DMI

COPENHAGEN 2001

ISSN 0905-3263
ISSN 1399-1949 (online)
ISBN 87-7478-433-1

Radioholographic methods for processing radio occultation data in multipath regions

M. E. Gorbunov
Atmosphere Ionosphere Research Division
Danish Meteorological Institute, 2100 Copenhagen, Denmark

18 December 2000

Abstract

Multipath propagation in the lower troposphere plays a very important role in forming the structure of radio signals used for radio occultations. Processing radio occultation data in multipath regions requires the solution of the problem of the reconstruction of the ray structure of a wave field. Two methods were formerly suggested for processing multipath data: back-propagation and radio-optic (radio-holographic or sliding-spectral) method. In the first section of this report we analyzed the two methods and their restrictions. Back-propagation method does not work in the presense of complicated caustic structures. The radio-optic method results in significant errors in sub-caustic zones. In the second section we suggest a combination of these methods. It uses the spectral analysis of both measured and back-propagated field and the computation of the averaged spatial spectra. It is shown that the effects of caustic are suppressed in the averaged spectra, which allows for the reconstruction of refraction angles. In the third section we suggest a new method of the reconstruction of the ray structure of a wave field. The method is based on the theory of canonical transforms and Fourier integral operators. It allows for a very accurate reconstruction of unique profiles of refraction angles. All the methods are validated in numerical simulations based on global field from analyses of European Centre for Medium-Range Weather Forecast.

1 Comparative analysis of radioholographic methods of processing radio occultation data

1.1 Introduction

Radio occultation sounding of the Earth's atmosphere using the radio signals of the Global Positioning System (GPS) can be a valuable source of information about key atmospheric variables [*Ware et al.*, 1996; *Rocken et al.*, 1997; *Kursinski et al.*, 1997]. The experience of processing data from the Microlab-1 satellite as well as theoretical considerations show that the most complicated problems of the interpretation

of radio occultation data arise in the lower troposphere [*Gorbunov et al.*, 1996b; *Gorbunov and Gurvich*, 1998a, b]. On the other hand, lower tropospheric data are of the greatest importance for numerical weather prediction (NWP). The difficulties of data processing can be classified as follows:

1. They can be classified as algorithmic problems. Processing the phase and amplitude measurements in multipath areas requires a special technique for the separation of interfering rays.

2. They can be classified as technical problems. The receiver used in the Microlab-1 satellite was not capable of tracking the signal with the strong amplitude and phase scintillations resulting from lower tropospheric inhomogeneities and multipath propagation, on the background of significant refractive attenuation of the signal. This resulted in the lack of reliable lower tropospheric data.

Two different approaches to processing radio occultation data in multipath areas have been discussed in the literature: (1) the analysis of spatial spectra, which we will refer to as the radio-optic method [*Lindal et al.*, 1987; *Pavel'ev*, 1998], and (2) the back propagation technique, which is also referred to as diffraction correction [*Marouf et al.*, 1986; *Gorbunov et al.*, 1996b; *Karayel and Hinson*, 1997; *Gorbunov and Gurvich*, 1998a, b]. Both methods can be termed radioholographic, because they are based on the analysis of records of complex radio signals, or radio holograms. In this section, we analyze their capabilities in processing data of GPS radio occultation sounding of the Earth's atmosphere.

Because of the lack of reliable lower tropospheric data our analysis can only be based on simulated radio occultations. The simulations were performed with global fields of pressure, temperature, and humidity from analyses of the European Centre for Medium-Range Weather Forecasts (ECMWF).

The results presented in this chapter are based on Ref. [*Gorbunov et al.*, 2000].

1.2 Radio Occultation Technique for Sounding Planetary Atmospheres

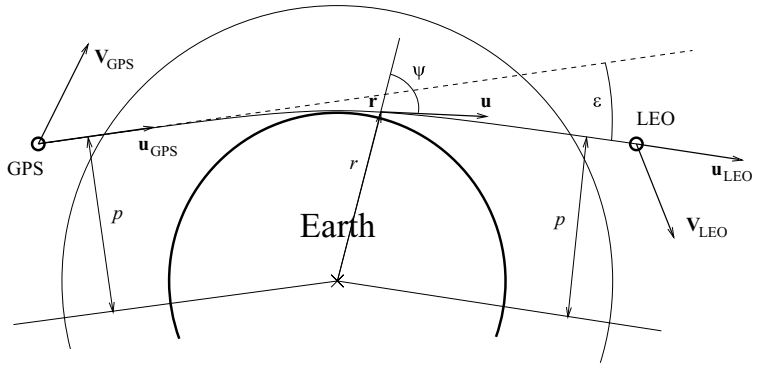

Figure 1: Radio occultation geometry.

The radio occultation technique is based on the transillumination of a planetary atmosphere with radio waves emitted by a spaceborne transmitter and received by a spaceborne receiver. In the sounding of the Earth's atmosphere the signal is transmitted by a GPS satellite and received by a low-Earth orbiter (LEO) equipped with a GPS receiver. The typical observation geometry is shown in Figure 1. During a (setting) occultation the satellites are moving in such a way that the radio ray connecting them immerses into the atmosphere until the receiver reaches the solid Earth's shadow or loses the signal earlier. The phase (or Doppler frequency) and amplitude of the received signal are recorded for their subsequent use for the reconstruction of atmospheric refractive index, which can be interpreted in terms of atmospheric variables [*Gorbunov et al.*, 1996a; *Ware et al.*, 1996; *Rocken et al.*, 1997; *Kursinski et al.*, 1997; *Steiner et al.*, 1999].

Basic approximations for the interpretation of radio occultation data are geometric optics and local spherical symmetry, which allows for the formulation of the inverse problem in terms of measured dependence of refraction (bending) angle ε versus impact parameter p. The vertical profile of atmospheric refractive index $n(r)$ must be reconstructed. In a spherically symmetrical medium, rays are plane curves, and impact parameter is a ray invariant such that at each point of the ray, $p = n(r) r \sin\psi = n(r) \mid \mathbf{r} \times \mathbf{u} \mid$, where ψ is the angle between local ray direction $\mathbf{u}$ and radius vector $\mathbf{r}$. This statement is referred to as Snell's law for a spherically symmetric medium or the formula of Bouger [*Born and Wolf*, 1964]. Using the relation between the measured Doppler frequency ω_{LEO} and the frequency of the transmitted signal ω_{GPS}, complemented with the vector form of Snell's law, we can write equations for the determination of ray directions $\mathbf{u}_{\mathrm{GPS}}$ and $\mathbf{u}_{\mathrm{LEO}}$ [*Fjeldbo et al.*, 1971; *Vorob'ev and Krasil'nikova*, 1994]:

$$\begin{gathered} \frac{c - \mathbf{V}_{\mathrm{LEO}} \cdot \mathbf{u}_{\mathrm{LEO}}}{c - \mathbf{V}_{\mathrm{GPS}} \cdot \mathbf{u}_{\mathrm{GPS}}} \sqrt{\frac{c^2 - V_{GPS}^2}{c^2 - V_{LEO}^2}} = \frac{\omega_{\mathrm{LEO}}}{\omega_{\mathrm{GPS}}}, \\ \mathbf{r}_{\mathrm{LEO}} \times \mathbf{u}_{\mathrm{LEO}} = \mathbf{r}_{\mathrm{GPS}} \times \mathbf{u}_{\mathrm{GPS}}, \end{gathered} \tag{1}$$

where c is the light velocity in a vacuum, $\mathbf{V}_{PS}$ and $\mathbf{V}_{EO}$ are the GPS and LEO velocities and $\mathbf{r}_{\mathrm{GPS}}$ and $\mathbf{r}_{\mathrm{LEO}}$ are the GPS and LEO positions. It is assumed that both satellites are in a vacuum.

The refraction angle can be calculated as angle ε between $\mathbf{u}_{\mathrm{GPS}}$ and $\mathbf{u}_{\mathrm{LEO}}$. Impact parameter p equals $|\mathbf{r}_{\mathrm{LEO}} \times \mathbf{u}_{\mathrm{LEO}}| = |\mathbf{r}_{\mathrm{GPS}} \times \mathbf{u}_{\mathrm{GPS}}|$. Dependence $\varepsilon(p)$ can be inverted using the Abel integral transform [*Phinney and Anderson*, 1968; *Fjeldbo et al.*, 1971], which is the exact solution for a spherically symmetrical field $n(r)$ but is also used as an approximation for real atmospheres with horizontal gradients of n.

Because Snell's law (the formula of Bouger) is violated in the real atmosphere with horizontal gradients ($|\mathbf{r}_{\mathrm{LEO}} \times \mathbf{u}_{\mathrm{LEO}}| \neq |\mathbf{r}_{\mathrm{GPS}} \times \mathbf{u}_{\mathrm{GPS}}|$), ε and p determined from (1) will not coincide with the real bending angle and impact parameter (the latter will be different at GPS and LEO) [*Ahmad and Tyler*, 1999]. Nevertheless, the dependence $\varepsilon(p)$ can be looked at as a known functional of the refractive in-

dex field and as such assimilated into global atmospheric circulation models using three-dimensional or four-dimensional variational assimilation techniques (3DVar or 4DVar) [*Eyre*, 1994; *Gorbunov et al.*, 1996a]. In this approach, (1) is looked at as the definition of the functional that can be applied without making the assumption of the spherical symmetry of the refracting medium. This approach avoids errors due to the approximation of the local spherical symmetry.

Equation (1) assumes single-ray propagation. A typical situation for the lower troposphere is, however, multipath propagation. Doppler frequency can be computed as the derivative of the phase of the wave field, also in a multipath area. Formal application of (1) results then in a characteristic oscillating pattern in the (ε, p) plane, which reflects the interference oscillations of the phase [*Gorbunov and Gurvich*, 1998b]. The resulting dependence $\varepsilon(p)$ proves ambiguous and cannot be used in inversion algorithms (inversion is usually preceded by some heuristic procedure of the elimination of ambiguities). We come thus to the problem of the determination of the ray structure of a wave field measured by a spaceborne GPS receiver.

1.3 Radio-optic Method

The radio-optic method was used for processing soundings of planetary atmospheres [*Lindal et al.*, 1987], and recently its application to GPS radio occultation data was suggested [*Pavel'ev*, 1998]. The method is based on the analysis of the local spatial spectra of the measured complex wave field. Local spectra are computed by Fourier analysis of the record of the complex field in small sliding apertures. Rays must correspond to maxima in the Fourier spectra. The limitations of this method will now be analyzed.

We shall use Cartesian coordinates (x, z) with the x axis pointing in the direction of the initial wave propagation and the z axis transverse to it. The (0,0) point of the coordinate frame is located in the Earth's local curvature center.

The wave field is observed at distance x from the Earth's limb, which is estimated as $\sqrt{r_{\mathrm{LEO}}^2 - r_E^2}$, where r_{LEO} is the LEO orbit radius and r_E is the Earth's local curvature radius. The spatial spectrum of the wave field is analyzed inside vertical apertures with size A. The angular resolution of the spatial spectrum can be estimated as λ/A. Assuming that the wave field can be described in the geometric optical approximation, we shall interpret this relationship in terms of refraction angles and impact parameters.

Each ray can be associated with a plane wave $\exp\left(i\sqrt{k^2 - k_z^2}x + ik_z z\right)$. Using the approximation of small refraction angle and infinitely remote GPS, we can write the following relationships for the refraction angle and impact parameter at observation point (x, z):

$$\begin{aligned} \varepsilon &= \frac{k_z}{k}, \\ p(x, z, \varepsilon) &= z + x\varepsilon. \end{aligned} \tag{2}$$

The second relationship can be rewritten as follows:

$$\varepsilon_G(x,z,p) = \frac{p-z}{x}, \tag{3}$$

which specifies the geometric relationship for the refraction angle and impact parameter of a ray coming to the observation point. In order to find all such rays we must solve the following equation:

$$\varepsilon_G(x,z,p) = \varepsilon(p). \tag{4}$$

The spectral resolution, $\Delta k_z = 2\pi/A$, determines the resolution of the refraction angle:

$$\Delta\varepsilon = \frac{\Delta k_z}{k} = \frac{\lambda}{A}. \tag{5}$$

On the other hand, the aperture size determines the resolution of the impact parameter:

$$\begin{aligned} \Delta p &= \left|\frac{dp}{dz}\right| A = \frac{A}{\zeta}, \\ \zeta &= \left|1 - x\frac{d\varepsilon}{dp}\right|. \end{aligned} \tag{6}$$

Because refraction angle and impact parameter must satisfy geometric relationship (3), their uncertainties can be estimated as follows:

$$\begin{aligned} \delta p^2 &= \Delta p^2 + x^2\Delta\varepsilon^2 = \frac{A^2}{\zeta^2} + \frac{x^2\lambda^2}{A^2}, \\ \delta\varepsilon^2 &= \Delta\varepsilon^2 + \frac{\Delta p^2}{x^2} = \frac{\lambda^2}{A^2} + \frac{A^2}{x^2\zeta^2}. \end{aligned} \tag{7}$$

These equations allow for the estimation of the optimal aperture size that minimizes both $\delta\varepsilon$ and δp:

$$A = \sqrt{\zeta x\lambda}. \tag{8}$$

The uncertainties of the refraction angle and impact parameter can then be estimated by their order of magnitude:

$$\begin{aligned} \delta\varepsilon &\approx \sqrt{\frac{\lambda}{\zeta x}}, \\ \delta p &\approx \sqrt{\frac{x\lambda}{\zeta}}. \end{aligned} \tag{9}$$

We have thus the uncertainty relation

$$\delta\varepsilon\,\delta p \sim \frac{\lambda}{\zeta}. \tag{10}$$

Because $d\varepsilon\,dp$ is the natural measure in the space of (straight-line) rays [*Santalo*, 1976], we can understand this relationship as the estimation of the volume of a quantum cell in this space. Two rays can be distinguished if they cannot be covered with one cell.

For the GPS radio occultations performed by the Microlab 1 satellite the observation distance was ~ 3000 km, and the wavelength ~ 20 cm. For weak refraction ($\zeta \approx 1$) the uncertainties of refraction angle and impact parameter are then estimated as 2.6×10^{-4} rad and 800 m, respectively. For the purposes of NWP we must reconstruct pressure with an accuracy of 1 mbar (0.1%), temperature with an accuracy of 1 K (0.3%), and geopotential heights with an accuracy of 10m. The accuracy of refraction angle in the lower troposphere is then estimated as 0.1%, or $\sim 3 \times 10^{-5}$ rad. The required accuracy of impact parameter must be ~ 10 m. Although the above estimations of the uncertainties exceed these values, we must not forget that multipath propagation is only significant in the lower troposphere, where ζ can be fairly large (30-300), and the uncertainties will be reduced by a factor of $\sqrt{\zeta}$. It must also be noted that the amplitude of the signal in the geometric optical approximation is also inversely proportional to $\sqrt{\zeta}$.

In the lower troposphere, where $\zeta \gg 1$, it can be approximately written $\zeta \approx |x\,d\varepsilon/dp|$. Parameter ζ is then proportional to the observation distance x, and from (9) it follows that the uncertainty of the refraction angle can be reduced by means of the forward propagation of the observed wave field to a plane located at a larger distance from the atmosphere. This equation, however, shows that this will not improve the uncertainty of the impact parameter, and thus the limitation of the vertical resolution will still persist. This shows that the overall uncertainty volume $\delta\epsilon\,\delta p$ is not so important as its shape.

The uncertainty relation is not the only restriction of the radio-optic method. Because it is based on the representation of the wave field in the form of a sum of waves corresponding to geometric optical rays, this method is incapable of taking diffraction effects into account.

The relation between the geometric optical approximation and the exact solution of the diffractive problem was already discussed in literature [*Kravtsov and Orlov*, 1990], and it was shown that these solutions are very close to each other everywhere

in a free space except subcaustic zones and the size of a subcaustic zone was estimated. The approach based on the theory of canonic operators [*Mishchenko et al.*, 1990] results in the same conclusion. This is also corroborated by the numerical simulations described in Section 5. Because the wave field in subcaustic zones cannot be interpreted in terms of geometric optical rays, the radio-optic method cannot be applied there.

As we shall see in Section 5, subcaustic zones (for GPS/MET observation geometry) are narrow enough to be excluded without resulting in a significant loss of data. On the other hand, the caustic structure is a priori unknown (knowledge of the caustic structure is equivalent to knowledge of $\varepsilon(p)$). At the moment we cannot formulate the algorithm of the identification of subcaustic zones for their exclusion.

1.4 Back Propagation Method

The back propagation method was first suggested for the profiling of Saturn's rings from diffracted images *Marouf et al.* [1986]. The method was initially designed to correct for the diffraction effects, which were significant in the interpretation of images of Saturn's rings recorded from a large observation distance.

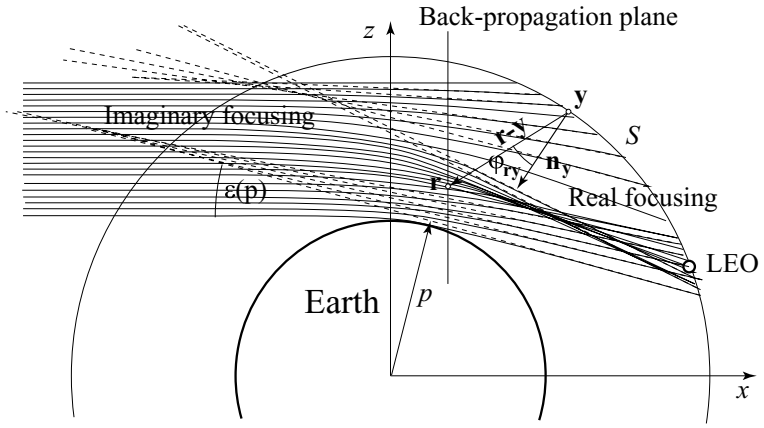

Figure 2: Multipath propagation geometry and back propagation. Nonmonotonous vertical profile $\epsilon(p)$ results in real focusing of rays and multipath propagations. Back propagation of the wave field (back-propagated rays are shown as dashed lines) results in imaginary focusings. Back-propagated field at point $\mathbf{r}$ is calculated via diffractive integral as a superposition of ininitesimal fields from the points of curve S. Each point $\mathbf{y}$ can be represented as a transmitter with intensity $u_0(\mathbf{y})$ and direction diagram $\cos\varphi_{\mathbf{ry}}$.

Recently the method was modified for processing radio occultation data in multipath areas [*Gorbunov et al.*, 1996b; *Karayel and Hinson*, 1997; *Hinson et al.*, 1997, 1998; *Gorbunov and Gurvich*, 1998a, a]. The method is based on the solution of the boundary problem for the Helmholtz equation in a vacuum, the boundary conditions being delivered by the measurements of the complex field along the LEO orbit. From the geometric optical viewpoint, this solution corresponds to the back

continuation of the rays as straight lines. Such a continuation conserves both ray direction (and therefore the refraction angle) and impact parameter. The field is back-propagated to some plane positioned, if possible, in a single-ray area (Figure 2).

The new feature of the method is that although the back propagation is performed as in a vacuum, the back propagation plane can (and must) be positioned inside the atmosphere, and the back-propagated field is thus not the real wave field at the location of the back propagation plane.

Assuming that the source of the wave field (GPS) is stationary and that the LEO orbit is located in a vertical plane, which we will refer to as the occultation plane, the back-propagated field is calculated using the diffractive integral [*Vladimirov*, 1971; *Gorbunov et al.*, 1996b]:

$$u(\mathbf{r}) = \left(\frac{k}{2\pi}\right)^{1/2} \int_S u_0(\mathbf{y}) \times \\ \times \cos\varphi_{\mathbf{ry}} \frac{\exp\left(-ik|\mathbf{r}-\mathbf{y}| + i\pi/4\right)}{|\mathbf{r}-\mathbf{y}|^{1/2}} dS_{\mathbf{y}}, \tag{11}$$

where $\varphi_{\mathbf{ry}}$ is the angle between vector $\mathbf{r}-\mathbf{y}$ and normal $n_{\mathbf{y}}$ to curve S at current integration point $\mathbf{y}$, and $u_0(\mathbf{y})$ is the boundary condition. Curve S is the LEO trajectory. Although real occultations are not vertical, it is possible to reduce the problem to the case where the GPS satellite is stationary, and the LEO satellite is moving vertically, by means of an appropriate coordinate transform *Gorbunov et al.* [1996b].

As discussed in Section 3, diffractive effects in single-ray areas are negligible. Therefore, if the back propagation plane is positioned in a single-ray area, then the back-propagated field can be interpreted in terms of geometrical optics. The Doppler frequency is calculated by means of the numerical differentiation of its phase. The refraction angles and impact parameters are then found by solving (1).

The calculation of Doppler frequency by means of the numerical differentiation of the phase can be performed with a much smaller effective aperture than that required for the radio-optic method. The wavenumber-aperture uncertainty relation does not apply here because of the use of a very strong assumption of single-ray propagation. This can be explained as follows: Given a complex wave field $u(z)$, the uncertainty relation states that $\delta k_z\, \delta z \geq 2\pi$, where δz is the aperture size and δk_z is the spectral resolution. If the spatial spectrum is grouped around some frequency $k_z^{(0)}$, then for an aperture size approximately equal to the oscillation period of the wave field, $2\pi/k_z^{(0)}$, the spatial spectrum cannot be determined, because $\delta k_z \geq k_z^{(0)}$. The situation is different if it is a priori known that the field is measured in a single-ray area. It can then be represented in the form $u(z) = a(z)\exp\left[i\int k_z(z)dz\right]$, where amplitude $a(z)$ and spatial frequency $k_z(z)$ are very slowly changing inside an oscillation period. In this case the frequency can be accurately calculated from the oscillation period, and wave vector $\mathbf{k}(z) = \left[\sqrt{k^2 - k_z^2(z)},\, k_z(z)\right]$ points in the direction of the single ray at a given point.

The basic restriction of the back propagation method is related to the configuration of rays and caustics of the back-propagated field in the occultation plane, which

will now be investigated. The straight line associated with a ray characterized by refraction angle ε and impact parameter p is described by the following equation:

$$x \sin \varepsilon(p) + z \cos \varepsilon(p) = p. \tag{12}$$

A caustic is the envelope of the family of rays. In the simplest cases each caustic is the boundary between multipath and single-ray propagation areas. The equation for caustics is derived by complementing (12) with its derivative with respect to parameter p *Korn and Korn* [1968]. Solving the resulting system, we arrive at the equations for caustics:

$$\begin{aligned} x &= p \sin \varepsilon(p) + \frac{\cos \varepsilon(p)}{\varepsilon'_p(p)}, \\ z &= p \cos \varepsilon(p) - \frac{\sin \varepsilon(p)}{\varepsilon'_p(p)}. \end{aligned} \tag{13}$$

Assuming that $|\varepsilon'_p(p)| < \infty$, we see that the complete envelope can be represented as a set of continuous caustics corresponding to the monotonous fragments of the dependence $\varepsilon(p)$. They can be subdivided into two classes: real caustics with $\varepsilon'_p(p) > 0$ arising because of focusing of rays in the observation plane, and imaginary caustics with $\varepsilon'_p(p) < 0$ arising because of defocusing (or imaginary focusing).

Equation (13) indicates that each ray with a p such that $\varepsilon'_p(p) \neq 0$ touches only one caustic (real or imaginary according to the sign of $\varepsilon'_p(p)$). The perigee points of the rays defined by the equations

$$\begin{aligned} x &= p \sin \varepsilon(p), \\ z &= p \cos \varepsilon(p) \end{aligned} \tag{14}$$

are located between real and imaginary caustics, and thus they are in a single-ray area. This suggests back-propagating the measured wave field to this curve. This solution is, however, associated with algorithmic difficulties, because the dependence $\varepsilon(p)$ itself must yet be determined, and iterations are thus necessary. Additional difficulties will also result from the complicated shape of such a curve. Currently, we back-propagate the measured field to a vertical straight line, whose position x can be estimated from (14) as $x = r_E \varepsilon_{\max}$ where the maximum refraction angle can be estimated from the processing of the measurements without back propagation. In most cases this estimation is sufficient for disentangling multipath ray structures. Other practical criteria for the right choice of the back propagation plane position can be the following.

1. There are minimum amplitude fluctuations of back-propagated field *Karayel and Hinson* [1997]. This criterion is based on the fact that the strongest amplitude fluctuation arise due to interference in multipath areas.

2. There is a minimum difference of optical path in L1 and L2 frequency channels. This criterion uses the strong frequency dependence of interference effects in multipath areas, while in one ray areas the frequency dependence of optical path can only be due to diffraction effects, which are very weak in single-ray areas for GPS/MET observations.

The situation becomes more complicated in the presence of a superrefraction layer. In this case the geometric optical dependence $\varepsilon(p)$ is characterized by a very sharp peak, where formally $|\varepsilon'_p(p)| = \infty$. As seen from (13), the caustic structure will then contain real and imaginary caustics very close to each other. In such cases the back propagation plane will always have intersections with caustics. Refraction angle profiles with sharp spikes caused by superrefraction or conditions approaching superrefraction constitute the basic limitation of the back propagation method.

As we have already seen, however, strong refraction resulting in large values of ζ is most favorable for the radio-optic method. This suggests combining the two methods for processing lower tropospheric data.

1.5 Numerical Simulations

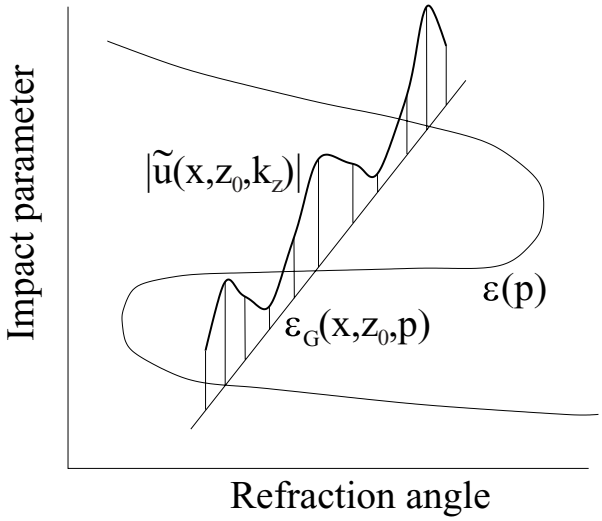

Figure 3: Geometry of the calculation of spatial spectra. Each ray is represented as a point in the (ϵ, p) plane. Each observation point (x, z_0) is represented as curve $\epsilon_G(x, z_0, p)$. Each spatial frequency k_z corresponds to point $(\epsilon(x, z_0, k_z), p(x, z_0, k_z))$ of this curve. Rays coming to given point are defined by the equation $\epsilon_G(x, z_0, p) = \epsilon(p)$. Absolute values of the spatial spectra of wave field $|\tilde{u}(x, z_0, k_z)|$ must have maxima corresponding to rays.

In the numerical simulations we compared the results of processing artificial occultation data using the back propagation and radio-optic methods. The artificial data were generated using the split-step numerical solution of the diffraction problem in the atmosphere [*Martin*, 1992; *Karayel and Hinson*, 1997; *Gorbunov and Gurvich*, 1998b]. The model of the atmospheric refractive index field was based on the global

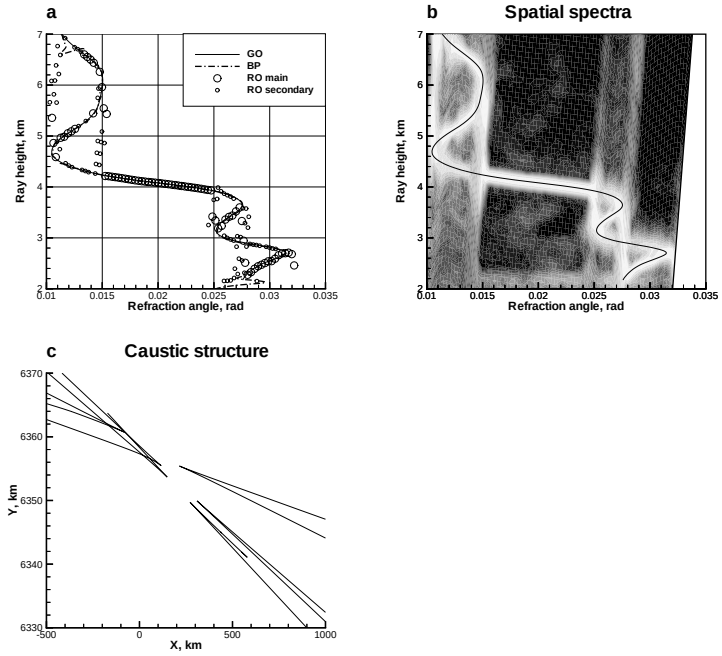

Figure 4: Simulated occultation event 0478 (February 2, 1997, 1637 UTC) at 29.3°S 173.0°E: a) refraction angle profiles (1) geometric optical (GO), (2) from back-propagated field (BP), (3) from phase measured at LEO, and (4) spectral maxima from radio optical analysis (RO); b) local spatial spectra in ray coordinates in pseudo-colour; c) caustic structure.

fields of temperature, humidity, and pressure from analyses of ECMWF. The occultation geometry was taken from real GPS/MET occultations and transformed to vertical occultation planes. The analysis fields are given with a time step of 6 hours; the analysis nearest to the time of the GPS/MET occultation event was chosen.

Using the geometric optical solution, we calculated the caustic structure, which allowed for the determination of the optimal position of the back propagation plane. The radio-optic method was applied to the complex field forward-propagated to a plane located at $x = 5000$km, which allowed for a slight improvement of the resolution. The forward-propagation plane was covered by sliding apertures with a size of $\sqrt{\zeta x \lambda}$. Factor ζ was evaluated from (6), where $\varepsilon(p)$ was computed from the observed phase with a very strong smoothing. In our simulation the accuracy of this estimation was sufficient. The basic sliding step of the sliding apertures was ~ 1.5 km.

Inside an aperture centered at z_0 the (forward propagated) complex field $u(z)$ was represented in the form

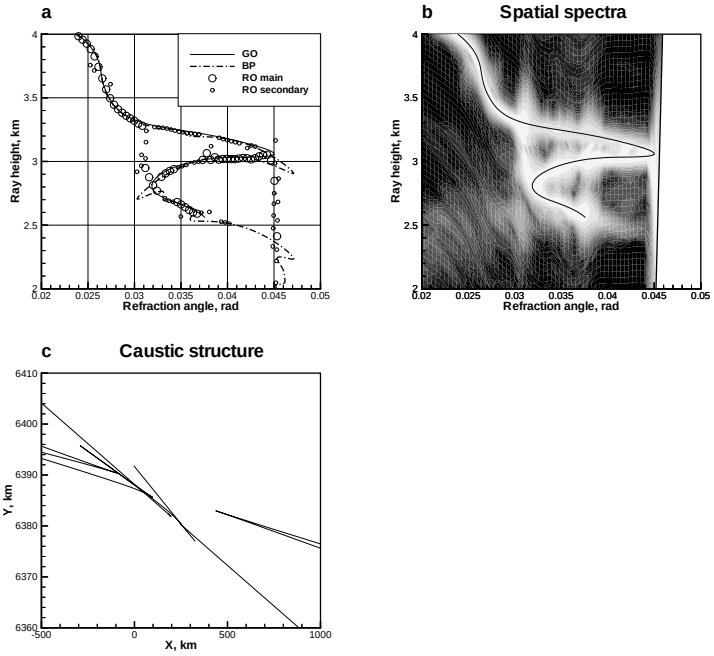

Figure 5: Simulated occultation event 0681 (February 2, 1997, 2342 UTC) at 29.1°S 171.4°W: a) refraction angle profiles (1) geometric optical (GO), (2) from back-propagated field (BP), (3) from phase measured at LEO, and (4) spectral maxima from radio optical analysis (RO); b) local spatial spectra in ray coordinates in pseudo-colour.

$$\begin{aligned} u(z) &= a(z)\exp\left(i\varphi(z)\right) \\ \varphi(z) &= \alpha_0 + \alpha_1(z-z_0) + \\ &\quad + \alpha_2(z-z_0)^2 + \Delta\varphi(z) \end{aligned} \tag{15}$$

where $a(z)$ is the amplitude, $\varphi(z)$ is the accumulated phase, and α_i are the regression coefficients. The complex field $a(z)\exp\left[i\Delta\varphi(z)\right]$ with downconverted spatial frequency was subjected to the Fourier analysis. This procedure approximately corresponds to the representation of the wave field $u(z)$ as a sum of spherical waves, and the square phase term in (15) approximately corrects for the wave front curvature. The discretization step Δz was chosen to be equal to $\lambda/\Delta\varepsilon \approx 200$ m, where $\Delta\varepsilon = 0.001$ rad is the a priori estimation of the width of the angular spectrum.

Downconverted frequencies σ_z correspond to spatial frequencies $k_z = \alpha_1 + \sigma_z$ of the initial field $u(z)$ in the center of the aperture. The wave vector is then equal to $\mathbf{k} = (k_x, k_z) = \left(\sqrt{k^2 - k_z^2}, k_z\right)$. Using Snell's law, we can compute refraction angles $\varepsilon(x, z_0, k_z)$ and impact parameters $p(x, z_0, k_z)$ corresponding to the ray direction of wave vector $\mathbf{k}$. This defines a mapping of (z_0, k_z) to (ε, p). For fixed observation point (x, z_0), dependencies $\varepsilon(x, z_0, k_z)$ and $p(x, z_0, k_z)$ are the parametric representation

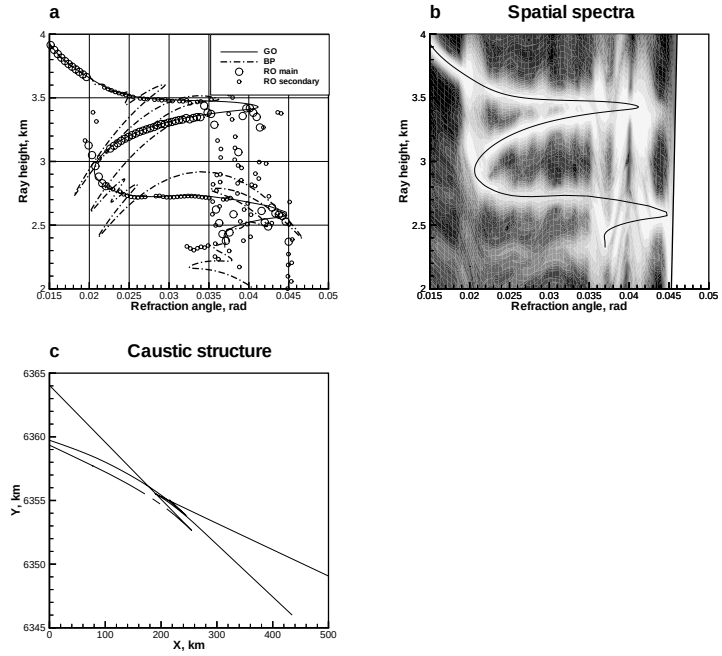

Figure 6: Simulated occultation event 0353 (February 7, 1997, 1236 UTC) at 18.0°N 177.3°W: a) refraction angle profiles (1) geometric optical (GO), (2) from back-propagated field (BP), (3) from phase measured at LEO, and (4) spectral maxima from radio optical analysis (RO); b) local spatial spectra in ray coordinates in pseudo-colour.

of curve $\varepsilon_G(x, z_0, p)$ in the (ε, p) plane, where k_z is the curve parameter. Each local spatial spectrum $\widetilde{u}(x, z_0, k_z)$ can then be plotted along this curve in (ε, p) coordinates. For all possible z_0, curves $\varepsilon_G(x, z_0, p)$ cover the complete (ε, p) plane, and the maxima of the spectra must thus trace the dependence $\varepsilon(p)$.

This is schematically shown in Figure 3, where dependencies $\varepsilon_G(x, z_0, p)$ and $\varepsilon(p)$ have three intersections, i.e. three rays interfere at a given observation point, and three maxima must be expected for absolute values of spatial spectrum $|\widetilde{u}(x, z_0, k_z)|$.

An example of processing artificial occultation data using the back propagation and radio-optic methods is shown in Figure 4. We computed the geometric optical refraction angles $\varepsilon_{\rm GO}(p)$ by means of the standard ray-tracing technique *Gorbunov et al.* [1996a]. Using them as the exact solution, we validate the back propagation and the radio-optic methods. Panel (a) of Figure 4 shows refraction angle profiles: (1) geometric optical $\varepsilon_{\rm GO}(p)$, (2) $\varepsilon_{\rm BP}(p)$ computed from back-propagated field, (3) $\varepsilon_{\rm LEO}(p)$ computed from phase measured at LEO, and (4) spectral maxima from radio optical analysis. Instead of impact parameter we use the ray leveling height defined as $p - r_E$. Panel (b) shows the local spatial spectra in ray coordinates in pseudo-colour. Panel (c) shows the configuration of caustics of the back-propagated wave field. The back propagation plane can be located between the real and imaginary caustics at $x = 200$ km. For the radio-optic analysis, factor ζ was estimated at 60, which corresponds to aperture size $A = 8$ km.

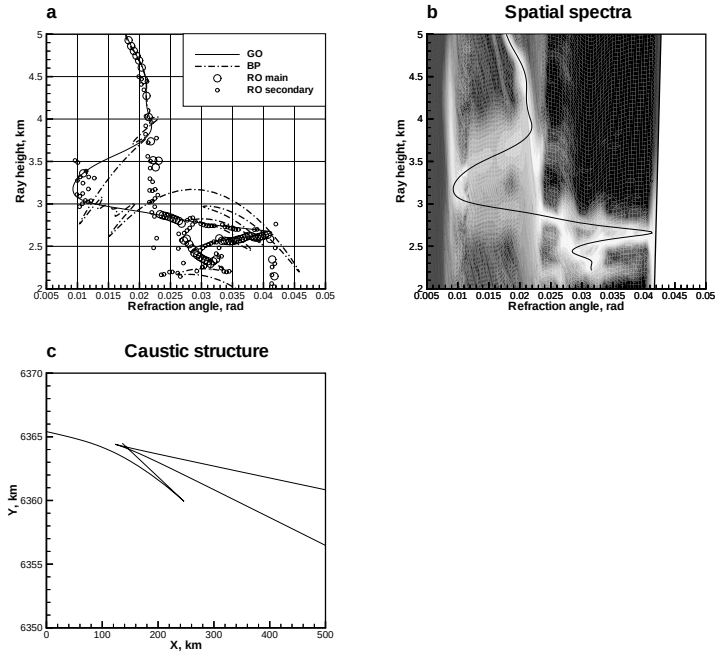

Figure 7: Simulated occultation event 0504 (February 7, 1997, 1754 UTC) at 39.4°S 156.6°E: a) refraction angle profiles (1) geometric optical (GO), (2) from back-propagated field (BP), (3) from phase measured at LEO, and (4) spectral maxima from radio optical analysis (RO); b) local spatial spectra in ray coordinates in pseudo-colour.

The multipath regions are marked with strong oscillations of the dependence $\varepsilon_{\rm LEO}(p)$, which becomes ambiguous there. The oscillations are concentrated near the branch of the dependence $\varepsilon_{\rm GO}(p)$ corresponding to the strongest of the interfering rays. Spectral maxima computed in the radio-optic method show a good agreement with $\varepsilon_{\rm GO}(p)$ everywhere, except in relatively narrow vicinities of the caustics, where diffraction effects are significant and spectral maxima cannot be interpreted in terms of rays. The best agreement with the exact solution is indicated by the back propagation method.

Figure 5 show another example of an artificial radio occultation, where the back propagation method is not so successful in the lowest troposphere. The caustic structure shown in Figure 5 is very characteristic for a superrefraction layer. No positioning of the back propagation plane can get rid of multipath propagation. For the radio-optic method, the value of ζ was estimated to be 215, which corresponds to aperture size $A = 15$ km. The vertical profile of refraction angles is characterized by a sharp spike at height of ~ 3 km. This spike is responsible for the real and imaginary caustic with overlapping projections to the x axis. For ray heights below 3.5 km the back propagation method proves incapable of reconstructing the true ray structure. The dependence $\varepsilon(p)$ is ambiguous here. This ambiguity, however, can serve as the indication that the back propagation plane intersects caustics and the back propagation method is inapplicable. Such a situation can also be diagnosed

by the amplitude fluctuations [*Karayel and Hinson*, 1997]. For this occultation the radio-optic method yields a much better agreement of the reconstructed ray structure with the exact geometric optical solution. However, the problem of extra spectral maxima in subcaustic areas remains unsolved. Figures 6 and 7 show further examples of occultations with complicated caustic structures.

1.6 Conclusions

The presented analysis allows for the following comparative characterization of the back propagation and radio-optic methods. The radio-optic method has two basic limitations.

1. One limitation is the uncertainty relation of refraction angle and impact parameter. The uncertainties, however, decrease in the lowest troposphere under the conditions of strong refraction, where the limitation of the resolution becomes less significant and thus the biggest impact of this method is expected.

2. Diffractive effects in subcaustic zones result in "false" maxima of the spatial spectra of the wave field, i.e., maxima that cannot be interpreted in terms of rays. Sorting out these maxima can become an important problem, especially with complicated profiles of refraction angles which can be expected in the lower troposphere.

The basic limitation of the back propagation method is related to complicated caustic structures, which can arise in the presence of strong refraction or superrefraction. Because strong refraction reduces the uncertainties of refraction angle and impact parameter in the radio-optic analysis, these two methods can be combined.

The basic advantage of the back propagation method is its high accuracy in the reconstruction of the profile of refraction angle when it is possible to position the back propagation plane in a single-ray area. However, even when it is impossible, this situation can at least be diagnosed by ambiguities in the dependence $\varepsilon(p)$ or by severe amplitude fluctuations in the back propagation plane.

2 Radioholographic analysis of radio occultation data in multipath zones

2.1 Introduction

Numerical simulations of GPS radio occultation experiments show that the effects of multipath propagation must play a significant role in the lower troposphere *Gorbunov and Gurvich* [1998b]; *Gorbunov et al.* [2000]. Two techniques for processing radio occultation data in multipath regions were discussed in the literature: (1) the back propagation method *Gorbunov et al.* [1996b]; *Hinson et al.* [1997]; *Gorbunov and Gurvich* [1998a, a]; *Hinson et al.* [1998] and (2) the radio optic (or radioholographic) method *Lindal et al.* [1987]; *Pavel'ev* [1998].

The former method consists in the numerical back propagation of the wave field recorded during a radio occultation experiment to a signle-ray region. The latter

method is based on the analysis of local spatial spectra of the wave field, where the spectral maxima are interpreted as rays.

The analysis of both mehtods *Gorbunov et al.* [2000] indicates that they have their restrictions. The back propagation method does not work for complicated caustic structures. The radio optic method cannot locate rays in the sub-caustic zones, where the wave field cannot be described in terms of geometric optics. The radio optic method has also a limited resolution. This restriction, however, is not very significant in the lower troposphere.

In this section we suggest a combination of both methods, which can be used for processing radio occultation data in multipath regions in the situations with complicated caustic structures. The combined method is based on the radio optic analysis of both the wave field recorded at the LEO orbit and the back-propagated field. The two local spatial spectra are computed in the ray coordinates (refraction angle and impact parameter), and the averaged spectrum is the computed. Then we localize the main maxima of the averaged spectra for each impact parameter. The refraction angle coordinates of the maxima trace the dependence of refraction angle versus impact parameter.

The method is validated on the material of global fields of atmospheric variables from analyses of the European Centre for Medium Range Weather Forecast (ECMWF).

The results presented in this chapter are based on an article submitted to *Radio Science*.

2.2 Data Analysis

The back propagation method is used in order to correct for the effects of multipath propagation [*Gorbunov et al.*, 1996b; *Hinson et al.*, 1997; *Gorbunov and Gurvich*, 1998a, b; *Hinson et al.*, 1998]. It uses the solution of the boundary problem of the Helmholtz equation in a vacuum. In this technique the complex wave field recorded along the LEO orbit during a radio occultation experiment is numerically back-propagated to a virtual observation plane located inside the atmosphere. From the geometric optical viewpoint this corresponds to the back continuation of the rays as straight lines, which often allows for disentangling the multipath structure.

The dependence of refraction angle ϵ versus impact parameter p defines a configuration of straight back-propagated rays and corresponding caustics. There are two classes of caustics: real and imaginary ones [*Gorbunov et al.*, 2000], and the back-propagation plane must be positioned in the single-ray area between them. If this is possible, then the back-propagation method provides a high accuracy in the reconstruction of refraction angle profiles. In the presense of strong refraction or superrefraction, however, structures with overlapping real and imaginary caustics can arise. In this case none positioning of the back-propagation plane can get rid of multipath propagation.

Another problem with this method is the choise of the back propagation plane position. This position depends on the caustic structure, which is a priori unknown.

An alternative technique of processing radio occultation data in multipath areas is the radio-optic method [*Lindal et al.*, 1987; *Pavel'ev*, 1998]. It is based on the

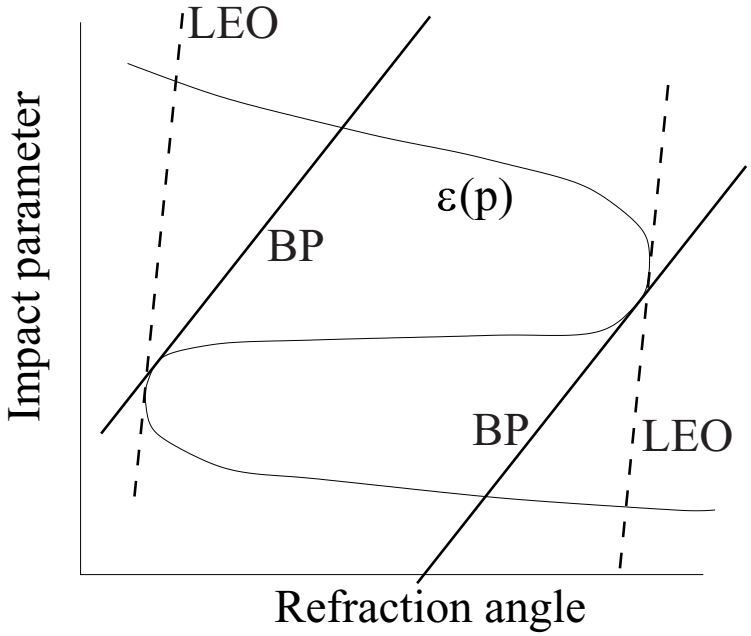

Figure 8: Geometry of calculation of spatial spectra. Thick dashed lines (LEO) represent two intersections of LEO orbit with caustics; thick solid lines (BP) represent two intersections of the back-propagation plane with caustics.

analysis of local spatial spectra of the recorded complex field in small sliding apertures. Rays correspond to the maxima of the spectra. This method, however, does not work in sub-caustic zones, where the wave field cannot be described in terms of geometric optics.

In this section we describe an improved approach to the radio-optic analysis based on combining it with the back-propagation.

We assume a vertical occultation with an immovable GPS. In the occultation plane we introduce cartesian coordinates x, z. Given an observation point at the LEO orbit, the radio-optic method locates the rays at this point using the Fourier analysis of the complex field in a surrounding aperture. Rays coming to a fixed observation point (x, z) must satisfy the geometric relationship:

$$x \sin \epsilon + z \cos \epsilon = p. \tag{16}$$

In the ray coordinates ϵ, p this equation specifies a curve representing the observation point. Each spatial frequency of the complex field corresponds to a ray direction at the observation point. Thus it specifies a ray with ε, p coordinates satisfying relationship (16). This means that each spatial frequency can be represented as a point of this curve. The spatial spectra of the recorded complex field can thus be plotted in the ray coordinates [*Gorbunov et al.*, 2000]. The maxima of the spectra must then trace the dependence $\epsilon(p)$.

For an observation point located on a caustic or in a sub-caustic zone, however, the spectral maxima cannot be interpreted in terms of rays. The spectrum will then

contain "false" maxima. If we represent the observation point with a corresponding curve in the ray coordinates, then the false maxima will be located along this curve.

The slope of curve (16) can be estimated as the observation distance x. This means that when the back-propagated wave field is subjected to the radio-optic analysis, then the locations of "false" maxima will be different as compared to the analysis of the field recorded at the LEO orbit. The situation is schematically shown in Figure 8

We use the following data analysis algorithm. We compute the logarithmic spatial spectra $\tilde{u}_{\rm LEO}(\epsilon, p)$ and $\tilde{u}_{\rm BP}(\epsilon, p)$ of the wave field at the LEO orbit and in the back propagation plane, respectively. For this purpose, the spatial spectra $\tilde{u}_{\rm LEO}(\epsilon, p)$ and $\tilde{u}_{\rm BP}(\epsilon, p)$ computed along different curves (16) are interpolated to a standard rectangular p-ε grid. Then we compute the averaged spatial spectrum:

$$\tilde{u}(\epsilon, p) = \frac{1}{2}\left(\tilde{u}_{\rm LEO}(\epsilon, p) + \tilde{u}_{\rm BP}(\epsilon, p)\right). \tag{17}$$

For each fixed impact parameter p, we find the location $\epsilon(p)$ the main maximum of the cross section of the spectrum $\tilde{u}(\epsilon, p)$. This specifies the dependence $\epsilon(p)$.

2.3 Numerical Simulations

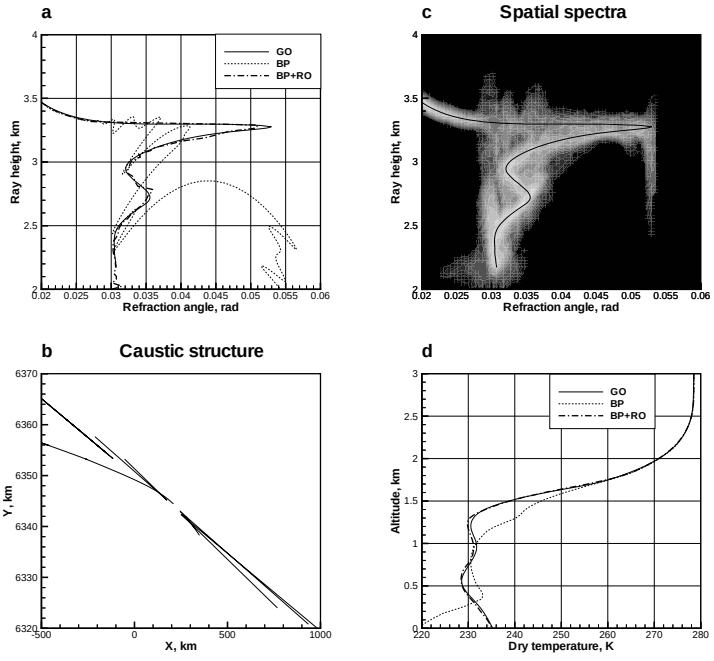

Figure 9: Occultation 0308, February 02, 1997: a) refraction angles: (GO) geometric optical, (BP) back propagation, and (BP+RO) combined algorithm; b) caustic structure; c) averaged spatial spectra; d) reconstrcuted temperatures.

In the numerical simulations we processed a few artificial occultation data sets. The artificial data were generated for the locations of real GPS/MET occultation

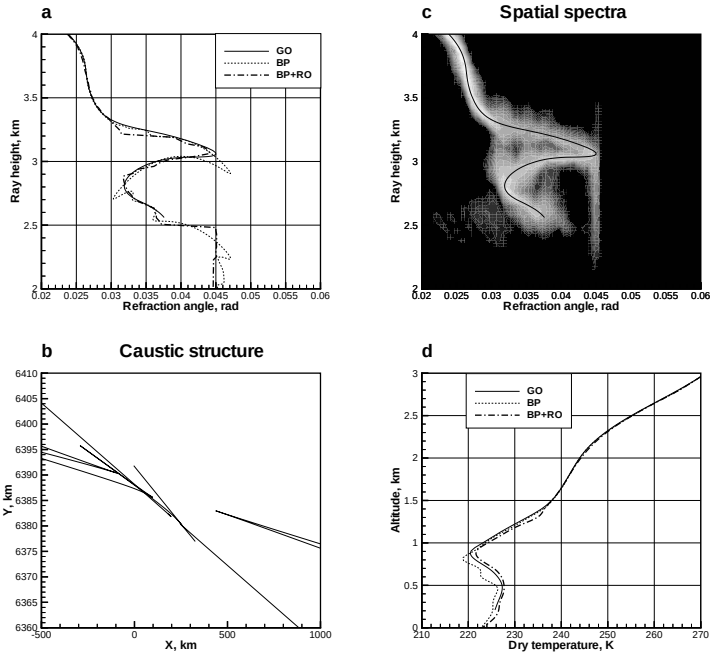

Figure 10: Occultation 0681, February 02, 1997: a) refraction angles: (GO) geometric optical, (BP) back propagation, and (BP+RO) combined algorithm; b) caustic structure; c) averaged spatial spectra; d) reconstrcuted temperatures.

events using global fields of atmospheric variables from analyses of the ECMWF. We used the wave optics model [*Gorbunov and Gurvich*, 1998b] for generating the artificial data. We also computed the refraction angles using the geometric optical ray equations, which were treated as the exact solution. We chose the occultation events with complicated caustic structures, where the back propagation method is inapplicable.

Figures 9, 10, and 11, show refraction angles, caustic structures, averaged local spatial spectra, and reconstructed temperature. We compare refraction angles computed using the geometric optics (GO), refraction angles computed using the back propagation method (BP), and refraction angles computed using the combined algorithm described above (BP+RO). For each refraction angle profile we compute corresponding dry temperature profile.

For the simulations we chose three occultations where the application of the back propagation method results in big errors in the reconstruction of the refraction angle profiles. This is the case if the refraction angle profiles have sharp spikes, which results in structures with overlapping real and imaginary caustics [*Gorbunov et al.*, 2000]. The combined radioholographic analysis, however, gives much better results. The error of reconstruction of the dry temperature using the radioholographic analysis is 0.5-1 K in all the examples. This error, however, reaches 10-20 K, when using the back propagation method.

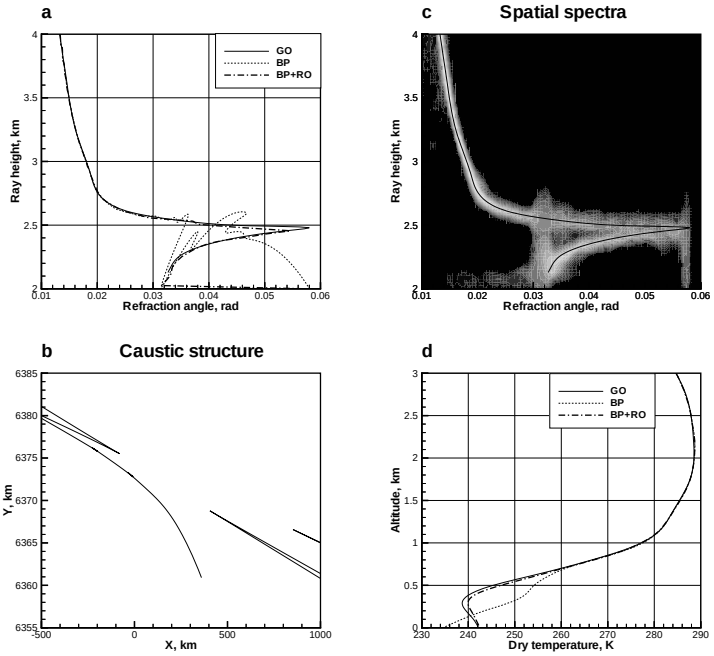

Figure 11: Occultation 0180, February 03, 1997: a) refraction angles: (GO) geometric optical, (BP) back propagation, and (BP+RO) combined algorithm; b) caustic structure; c) averaged spatial spectra; d) reconstrcuted temperatures.

2.4 Conclusions

Two methods of processing radio occultation data in multipath regions were previously suggested, which are (1) the back propagation method and (2) the radio optic method. It was also shown that both methods have their restrictions. The radio optic method cannot be applied in sub-caustic zones, where the diffraction effects are significant, and the wave field cannot be interpreted in terms of rays. On the other hand, the back propagation method cannot be applied for complicated caustic structures, which can arise if the refraction angle profile has sharp spikes.

We suggested the combination of the two methods. For this purpose, we compute the local spatial spectra of the wave field at the LEO orbit (observation plane) and of the back-propagated wave field. Both spectra are computed in the ray coordinates ε, p. For the averaged spectrum, we find its main maximum for each given impact parameter p. The positions of the main maximuma with respect to the ε coordinates traces the dependence $\varepsilon(p)$

The simulations showed that the combined algorithm can significantly improve the accuracy of the reconstruction of the refraction angles for the cases where the back propagation method does not work.

3 Canonical transform method for processing GPS radio occultation data in lower troposphere

3.1 Introduction

The interpretation of GPS radio occultation data in the lower troposphere is of a great importance for the incorporation of this type of data into numerical weather prediction models. The standard algorithm of processing radio occultation data involves the derivation of the dependence of refraction (bending) angle versus impact parameter, which is used for the formulation of the inverse problem in the geometric optical approximation [*Ware et al.*, 1996; *Rocken et al.*, 1997; *Kursinski et al.*, 1997]. The computation of refraction angles is straightforward in one-ray areas, where the derivative of the phase, or the Doppler frequency, can be related to the satellite velocities and ray directions at GPS and Low Earth Orbiter (LEO) satellites [*Vorob'ev and Krasil'nikova*, 1994]. Complementing this relation with Snell's law, one can derive the refraction angle and impact parameter from the Doppler frequency.

However, radio signals propagated through the lower troposphere can have a very complicated structure due to the effects of multipath propagation and diffraction [*Gorbunov et al.*, 1996b; *Gorbunov and Gurvich*, 1998b, b]. The refraction angle cannot be directly derived from the phase of wave field in multipath zones, because at each point the phase is defined by amplitudes and phases of multiple interfering rays. This results in the formulation of the problem of the determination of the ray structure of wave field.

Two methods were suggested for processing radio occultation signals in multipath zones: (1) back-propagation method [*Gorbunov et al.*, 1996b; *Karayel and Hinson*, 1997; *Hinson et al.*, 1997, 1998; *Gorbunov and Gurvich*, 1998a, a] and (2) radio-optic (or radiohолographic) method [*Lindal et al.*, 1987; *Pavel'ev*, 1998; *Hocke et al.*, 1999]. Both of them are based on simple physical considerations. The comparative analysis of the two methods performed by *Gorbunov et al.* [2000] indicates that both methods have very strong restrictions of their applicability.

In the first method, the wave field measured along the LEO trajectory is used as the boundary condition for the back-propagating solution of the Helmholtz equation in a vacuum. The underlying ray structure of this back-propagated field may have two types of caustics: real and imaginary. There may be a one-ray area between them, where the back-propagated field can already be processed in the standard way. The difficulty with the application of this method is, however, that the position of the one-ray area is unknown a priori, because the caustic structure depends on the profile of refraction angle, which must yet be determined. Numerical simulations, which were performed on the material of global field of atmospheric parameters from analyses of European Medium-Range Weather Forecast Center (ECMWF) [*Gorbunov et al.*, 2000], show that complicated caustic structures with overlapping real and imaginary caustics may occur, which causes the back-propagation method to fail. It is also clear that the real atmosphere must contain small-scale inhomogeneities, which are not represented in numerical weather prediction models and which will result in still more complicated structures of wave field propagating through the

atmosphere.

The radio-optic method utilizes the analysis of spatial spectra of the wave field in small sliding apertures. It is assumed that each ray can be locally associated with a basic wave form such as a plane or a spherical wave. Then the maxima of local spatial spectra identify interfering rays. The most important disadvantage of this method is that it cannot be applied for the analysis of wave field in sub-caustic zones, where the wave field has a complicated structure and cannot be interpreted in terms of rays [*Gorbunov et al.*, 2000].

In this section, we suggest a new approach to the problem, based on the theory of Fourier integral operators. As shown in [*Mishchenko et al.*, 1990], a wave problem can be associated with a canonical Hamilton system, which describes the geometric optical ray structure of the wave field. The Hamilton system is written in terms of spatial coordinates and impact, the latter corresponding to the differential operator in the wave problem. On the other hand, coordinate vector and impact define the initial conditions of a ray. We can thus consider the manifold of all possible rays and introduce ray coordinates, which are impact parameter and refraction angle. We can also write a canonical transform [*Arnold*, 1978] mapping spatial coordinates and impact to ray coordinates. It can be shown that the impact parameter now plays the role of the spatial coordinate, while the refraction angle is the new impact. A Fourier integral operator can be associated with this canonical transform [*Egorov*, 1985]. This operator transforms the wave function to the representation of ray coordinates. The argument of the transformed wave function is now the ray impact parameter, and the derivative of its phase (the new impact) is the refraction angle. This method is applicable if an unique dependence of refraction angles versus impact parameter exists, which means that rays can be uniquely identified by their impact parameters.

We designed a fast numerical implementation of the method based on the FFT. For the validation of the new method we process simulated radio occultations, where the application of the back-propagation method results in big errors.

The results presented in this chapter are based on an article submitted to *Radio Science*.

3.2 Helmholtz Equation, Fourier Integral Operators, and Canonical Transforms

We shall use the direct and inverse 1D k-Fourier transform in the following definition:

$$\begin{aligned} \widetilde{f}(\xi) &= \int e^{-ikx\xi} f(x) dx, \\ f(x) &= \frac{k}{2\pi} \int e^{ikx\xi} \widetilde{f}(\xi) d\xi, \end{aligned} \tag{18}$$

where k is the wave vector. We shall also use differential operators like $D_x = \frac{1}{ik}\frac{\partial}{\partial x}$.

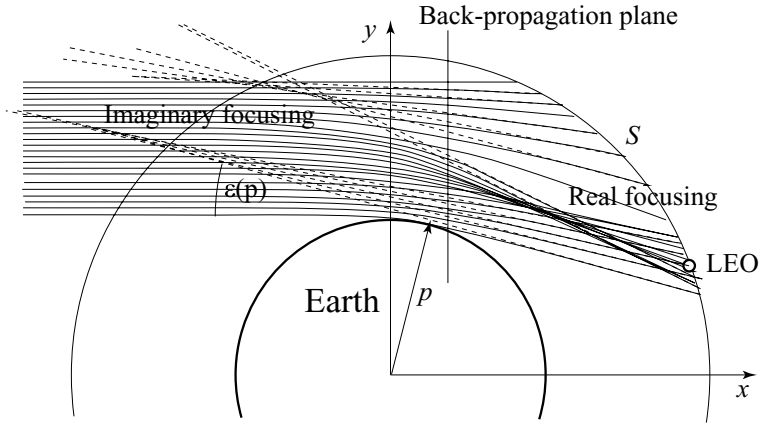

Figure 12: The geometry of multipath propagation.

We shall use Cartesian coordinates (x, y), where the x-axis points in the direction of the incident wave, and the y-axis is transversal to it. The geometry is shown in Figure 12. In a radio occultation experiment, the wave field propagated through the atmosphere is recorded along the LEO trajectory S. The recorded complex field can be back-propagated to some location x. From the geometric optical point of view, this procedure is equivalent to the continuation of rays backwards as straight lines. In the previous papers [*Gorbunov et al.*, 1996b; *Karayel and Hinson*, 1997; *Hinson et al.*, 1997, 1998; *Gorbunov and Gurvich*, 1998a, b] this method was applied in order to find the single-ray area between real and imaginary caustics. As was pointed out above, it is not always possible. Here we shall, however, always analyze the back-propagated field, because this procedure conserves impact parameters and refraction angles of rays. The back-propagation technique is thus an immanent part of the suggested method.

The back-propagated field $u(x, y)$ is described by the Helmholtz equation:

$$\left(-D_x^2 - D_y^2 + 1\right) u = 0. \tag{19}$$

The variable x can be looked at as time, because we consider the propagation of very short waves, and the backscattering can be neglected. Using the operator factorization of this equation [*Martin*, 1992], we can rewrite it in the following form:

$$\left(D_x + \sqrt{1 - D_y^2}\right) \left(-D_x + \sqrt{1 - D_y^2}\right) u = 0. \tag{20}$$

Assuming that the incident wave has the form $\exp(ikx)$, we can separate the equation for the forward propagating wave:

$$-D_x u = H(y, D_y)u \equiv -\sqrt{1 - D_y^2}u, \tag{21}$$

where $H(y, D_y)$ is the Hamilton operator, and $-D_x$ can be understood as the operator of energy. The Hamilton operator belongs to the class of pseudo-differential operators, which are defined as follows [*Egorov*, 1985]:

$$H(y, D_y)f = \frac{k}{2\pi} \int H(y, \eta) e^{iky\eta} \widetilde{f}(\eta) d\eta, \tag{22}$$

where the function $H(y, \eta)$ is the symbol of the operator. For big η, $|H(y, \eta)|$ must be majorated by $C\,|\eta|^m$, where m is called the order of the operator.

We shall use notation $u_x(y)$ for $u(x, y)$. Using the Fourier transform with respect to y, we can write the solution of the boundary problem *Zverev* [1975]

$$\widetilde{u}_x(\eta) = e^{ikx\sqrt{1-\eta^2}} \widetilde{u}_0(\eta). \tag{23}$$

The solution can thus be written in the form of a Fourier integral operator transforming function $u_0(y)$ to $u(z)$, and z is here a duplicate of the vertical coordinate:

$$u_x(z) = \frac{k}{2\pi} \int e^{ik\left[x\sqrt{1-\eta^2}+z\eta\right]} \widetilde{u}_0(\eta) d\eta. \tag{24}$$

A Fourier integral operator is defined as an operator of the following type [*Egorov*, 1985]:

$$\Phi u(z) = \frac{k}{2\pi} \int a(z, \eta) e^{ikS(z,\eta)} \widetilde{u}(\eta) d\eta, \tag{25}$$

where $a(z, \eta)$ is the symbol of the operator, and $S(z, \eta)$ is its phase function. Egorov's theorem [*Egorov*, 1985] states that this operator is associated with a canonical transform from the old coordinates (y, η) to the new coordinates (z, ξ) in the phase space. A canonical transform preserves the Hamilton structure in the phase space [*Arnold*, 1978]. For a transform to be canonical, the form $\eta dy - \xi dz$ must be a full differential, which is equivalent to the following condition [*Arnold*, 1978]:

$$y d\eta + \xi dz = dS(z, \eta). \tag{26}$$

where $S(z, \eta)$ is the generating function of the canonical transform from (y, η) to (z, ξ). And vice versa, given a function $S(z, \eta)$, we can write equations defining a canonical transform [*Arnold*, 1978]:

$$\begin{aligned} y &= \frac{\partial S(z, \eta)}{\partial \eta}, \\ \xi &= \frac{\partial S(z, \eta)}{\partial z}. \end{aligned} \tag{27}$$

If we now consider a Fourier integral operator with the phase function $S(z,\eta)$, then Egorov's theorem states that in the main order

$$\Phi Q = P\Phi, \tag{28}$$

where $Q = Q(y, D_y)$, $P = P(z, D_z)$ are pseudo-differential operators, whose symbols are related by the canonical transform with the generating function $S(z,\eta)$:

$$Q\left(\frac{\partial S(z,\eta)}{\partial \eta}, \eta\right) = P\left(z, \frac{\partial S(z,\eta)}{\partial z}\right). \tag{29}$$

This means that the operator Φ transforms the wave function from (y,η)-representation to (z,ξ)-representation. If we, for example, consider the function $S(z,\eta) = z\eta$, then the corresponding canonical transform is the identity: $y = z$, $\xi = \eta$, and the Fourier integral operator with phase function $S(z,\eta)$ and symbol $a(z,\eta) = 1$ is the composition of the direct and inverse Fourier transforms, which is also identity. The integral operator (24) corresponds to the canonical transform:

$$\begin{aligned} z &= y + \frac{\eta}{\sqrt{1-\eta^2}}x, \\ \xi &= \eta, \end{aligned} \tag{30}$$

which describes the evolution of straight rays with direction vectors $\left(\sqrt{1-\eta^2}, \eta\right)$. For negative x, this operator describes the back-propagation.

3.3 Canonical Transform to Ray Coordinates

We have by now introduced all the concepts necessary for the derivation of the Fourier integral operator transforming the wave function to the representation of the ray coordinates. First, we need to find the necessary canonical transform. We assume that rays can be identified by their impact parameters. Thus we can chose the new coordinate z to be equal to ray impact parameter: $z = -x\eta + y\sqrt{1-\eta^2}$.

For the definition of the new impact ξ we have the condition [*Arnold*, 1978]: $d\eta \wedge dy = d\xi \wedge dz$, which results in the equation:

$$\frac{\partial \xi}{\partial \eta}\frac{\partial z}{\partial y} - \frac{\partial \xi}{\partial y}\frac{\partial z}{\partial \eta} = 1 \tag{31}$$

If we assume that $\xi = \xi(\eta)$, then we have

$$\frac{\partial \xi}{\partial \eta} = \left(\frac{\partial z}{\partial y}\right)^{-1} = \frac{1}{\sqrt{1-\eta^2}}. \tag{32}$$

The canonical transform has thus the following form:

$$\begin{aligned} z &= -x\eta + y\sqrt{1-\eta^2}, \\ \xi &= \arcsin\eta, \end{aligned} \tag{33}$$

which indicates that the new impact ξ is the ray direction angle with respect to the x-axis. The generating function of this transform can be readily derived:

$$S(z,\eta) = z\arcsin\eta - x\sqrt{1-\eta^2} \tag{34}$$

The symbol of the Fourier integral operator can be chosen in the form [*Egorov*, 1985]:

$$a(z,\eta) = \left|\frac{\partial^2 S}{\partial z \partial \eta}\right|^{-1/2} = \left(1-\eta^2\right)^{1/4}. \tag{35}$$

This allows for writing the Fourier integral operator as follows:

$$\Phi u_x(z) = \frac{k}{2\pi}\int \left(1-\eta^2\right)^{1/4} e^{ik\left[z\arcsin\eta - x\sqrt{1-\eta^2}\right]}\widetilde{u}_x(\eta)d\eta \tag{36}$$

The transformed wave function $\Phi u_x(p)$ has the form $A(p)\exp\left(ik\int\xi(p)dp\right)$, where $A(p)$ is the amplitude. This allows for the computation of the impact as follows

$$\xi(p) = \frac{1}{k}\frac{d}{dp}\arg\Phi u_x(p) \tag{37}$$

Finally, the refraction angle is computed as follows:

$$\varepsilon(p) = -\xi(p) + \arcsin\left(\frac{|x_{GPS}| - \sqrt{x_{GPS}^2 - 2a\,(p-a)}}{a}\right),$$

where a is the Earth's radius, and the second term corrects for the ray direction angle at the GPS satellite.

An advantage of this method is that it allows for the computation of the refraction angle ε for a given ray impact parameter p, unlike the other methods, where ε and p are computed simultaneously for given point in the LEO trajectory or in the back-propagation plane, and noise may result in a non-unique function $\varepsilon(p)$.

3.4 Numerical Simulations

For the numerical simulations we used simulated occultation data computed for statistical comparisons of GPS/MET data and ECMWF analyses [*Gorbunov and Kornblueh*, 2001]. Figures 13 and 14 show the results of the simulations. The refraction

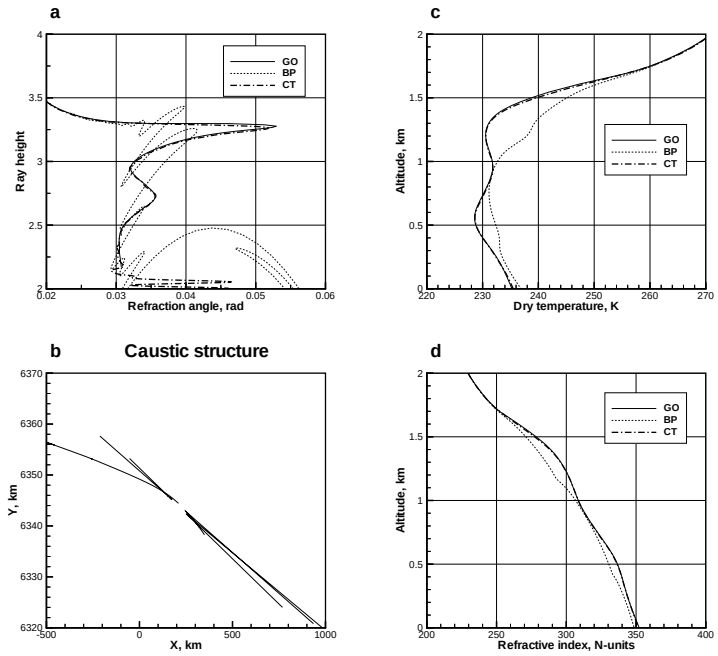

Figure 13: Simulated occultation 0308, February 02, 1997, UTC 10:41, 8.6°N 62.3°E: (a) refraction angles computed using geometric optical model (GO), back-propagation method (BP) and canonic transform (CT), (b) caustic structure of the back-propagated field, (c) reconstructions of dry temperature, and (d) reconstructions.

angles computed using the back-propagation and the canonical transform methods were compared with the geometric optical refraction angles, which were treated as the exact solution. In these examples, the application of the back-propagation method results in significant errors in the reconstruction of the refraction angle profiles in multipath zones. This is explained by the complicated caustic structure with overlapping real and imaginary caustics. The inversions of the refraction angle profiles computed by the back-propagation method indicate significant errors in the reconstructed profiles of refractivity and dry temperature. The canonical transform method, however, allows for a very accurate computation of the refraction angle profiles, which results in a high accuracy of inversions.

Figure 15 presents a simulated occultation, where strong horizontal inhomogeneities result in a non-unique dependence $\varepsilon(p)$. For a spherically symmetric medium, ray impact parameter is defined as $p = nr\sin\psi$, where ψ is the angle between the ray direction and local vertical. In a horizontally inhomogeneous medium this value is not constant. Its evolution along a ray is described by the dynamical equation [*Gorbunov et al.*, 1996a; *Kravtsov and Orlov*, 1990]:

$$\dot{p} = n\frac{\partial n}{\partial \theta}, \tag{38}$$

where θ is the polar angle in the occultation plane. This results in errors of the de-

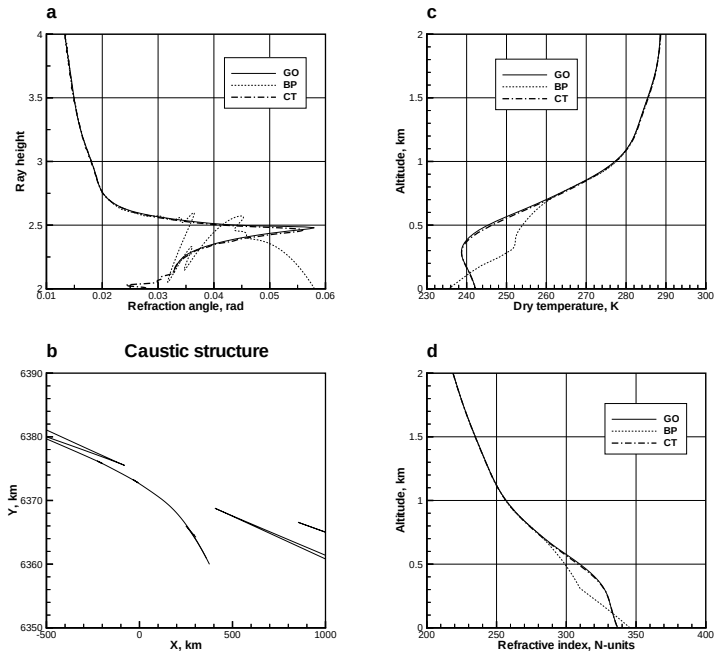

Figure 14: Simulated occultation 0180, February 03, 1997, UTC 06:22, 42.3°S 129.7°E: (a) refraction angles computed using geometric optical model (GO), back-propagation method (BP) and canonic transform (CT), (b) caustic structure of the back-propagated field, (c) reconstructions of dry temperature, and (d) reconstructions of refractivity.

termination of the effective refraction angle and impact parameter from the Doppler frequency in the assumption of spherical symmetry [*Ahmad and Tyler*, 1999]. This may also result in different rays having the same effective impact parameter. In this case the measured dependence $\varepsilon(p)$ is non-unique.

The variation of the ray impact parameter can be estimated as $a\Delta n$, where a is the Earth radius, and Δn is the variation of refractivity due to horizontal gradients along the ray. If we assume a 10 K variation of temperature and 3×10^{-3} kg/kg variation of specific humidity across an atmospheric front, then the horizontal variation of refractivity is about 30 N-units. The corresponding variation of the impact parameter is then about 200 m.

In Figure 15, the length of the impact parameter interval, where $\varepsilon(p)$ is non-unique is about 300 m, which is very close to the above estimation. In this interval, the transformed wave function $\Phi u_x(p)$ is approximately a superposition of three functions $A_j(p) \exp\left(ik \int \xi_j(p) dp\right)$ corresponding to multiple rays with the same impact parameters. Like in multipath zones, the computation of the refraction angle by means of the differentiation of the phase results in errors. The computed profile $\varepsilon(p)$ is mostly influenced by the strongest of the interfering rays. In this case the transformed wave function $\Phi u_x(p)$ can also be subjected to the spectral analysis in sliding apertures, like in the radio-optical method, which should reveal multiple branches of $\varepsilon(p)$.

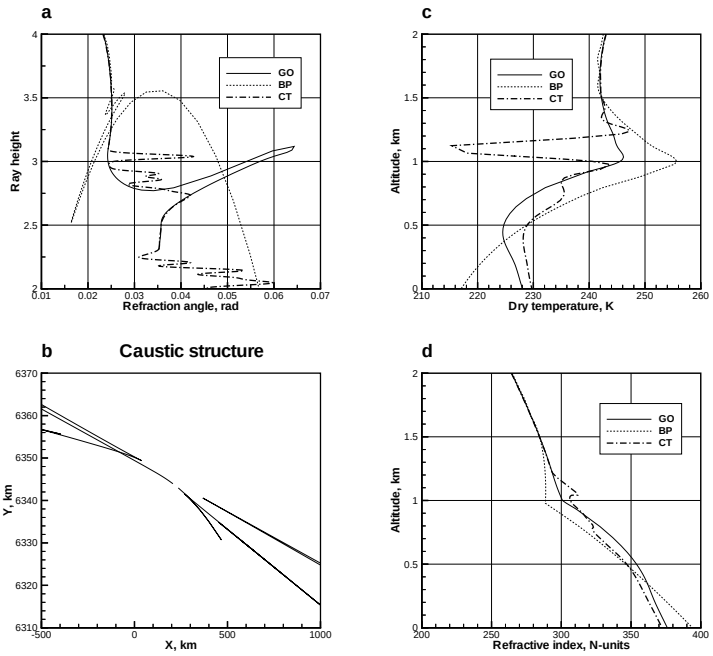

Figure 15: Simulated occultation 0052, February 05, 1997, UTC 01:48, 11.2°S 171.1°E: (a) refraction angles computed using geometric optical model (GO), back-propagation method (BP) and canonic transform (CT), (b) caustic structure of the back-propagated field, (c) reconstructions of dry temperature, and (d) reconstructions of refractivity.

3.5 Conclusions

In this section, we suggested a new approach to the problem of the computation of refraction angles from radio occultation data measured in multipath zones. The approach is based on the theory of Fourier integral operators. We consider the Helmholtz equation and the underlying Hamilton structure describing the rays of the geometric optical approximation for this equation. For this Hamilton structure we found the canonical transform mapping the spatial coordinate and impact to the ray coordinates. With this canonical transform we can associate a Fourier integral operator, which transforms the wave function from the representation of the spatial coordinates to the representation of the rays coordinates. In this representation, the wave function depends on the ray impact parameter, and the derivative of its phase is the refraction angle. If we assume that the rays can be uniquely identified by their impact parameters, then this method allows for disentangling the ray structure.

The limitation of the applicability of the canonical transform method is the requirement that the dependence of the refraction angle versus impact parameter should be unique. This condition can be broken in the presence of strong regular horizontal gradients of the atmospheric refractivity, which can be caused, for example, by atmospheric fronts. Such strong gradients, however, occur rarely. A possible solution for this situation could be the analysis of the spectra of the transformed wave function in small sliding apertures. On the other hand, in this case it is also

very difficult to formulate the inverse problem of atmospheric refraction, even if the exact refractivity profile is known.

The canonical transform method is an exact asymptotic solution of the problem of the reconstruction of the ray structure of a wave field. It allows for the reconstruction of unique dependencies of refraction angle versus impact parameter with a high accuracy. This method can be understood as a generalization of the back-propagation, which can also be written in the form of a Fourier integral operator associated with a canonical transform. However, the limits of the applicability of the canonical transform method are much wider than those of the back-propagation method.

4 Conclusions and Acknowledgements

This report is based on research performed prior to and during a visit to the Danish Meteorological Institute (DMI) as a visiting scientist from October to December 2000. This activity was sponsored by the GRAS Meteorology Satellite Application Facility (SAF) project.

The GRAS SAF is a Eumetsat development project hosted by DMI and with the two partner institutes the UK Met Office and IEEC in Spain. The scope of the GRAS SAF is to develop and set up a processing facility to deliver atmospheric parameters in real time that can be used for numerical weather prediction. The method is based on GPS satellite observations using the GRAS instrument onboard the Metop satellite.

The objective of this study was to focus on diffraction correction methods including the back propagation method and radio-optical (spectral) methods and to develop prototype algorithms for radio occultations with multipath propagation for use in the processing of the GRAS SAF products.

References

Ahmad, B., and G. L. Tyler, Systematic errors in atmospheric profiles obtained from abelian inversion of radio occultation data: effects of large-scale horizontal gradients, *J. Geophys. Res.*, *104*(D4), 3971–3992, 1999.

Arnold, V. I., *Mathematical methods of classical mechanics*, Springer-Verlag, New York, 1978.

Born, M., and E. Wolf, *Principles of optics*, Pergamon Press, New York, 1964.

Egorov, Y. V., *Lectures on partial differential equations. Additional chapters*, 1985.

Eyre, J. R., Assimilation of radio occultation measurements into a numerical weather prediction system, *Tech. Rep. Technical Memorandum No. 199*, European Center for Medium-Range Weather Forecast, 1994.

Fjeldbo, G., A. Kliore, and R. Eshleman, The neutral atmosphere of venus as studied with the mariner-5 radio occultation experiments, 1971.

Gorbunov, M. E., and A. S. Gurvich, Microlab-1 experiment: Multipath effects in the lower troposphere, *Journal of Geophysical Research*, *103*(D12), 13819–13826, 1998a.

Gorbunov, M. E., and A. S. Gurvich, Algorithms of inversion of Microlab-1 satellite data including effects of multipath propagation, *International Journal of Remote Sensing*, *19*(12), 2283–2300, 1998b.

Gorbunov, M. E., and L. Kornblueh, Analysis and validation of gps/met radio occultation data, *Journal of Geophysical Research*, 2001.

Gorbunov, M. E., S. V. Sokolovskiy, and L. Bengtsson, Space refractive tomography of the atmosphere: modeling of direct and inverse problems, *Tech. Rep. Report No. 210*, Max-Planck Institute for Meteorology, Hamburg, 1996a.

Gorbunov, M. E., A. S. Gurvich, and L. Bengtsson, Advanced algorithms of inversion of GPS/MET satellite data and their application to reconstruction of temperature and humidity, *Tech. Rep. Report No. 211*, Max-Planck Institute for Meteorology, Hamburg, 1996b.

Gorbunov, M. E., A. S. Gurvich, and L. Kornblueh, Comparative analysis of radioholographic methods of processing radio occultation data, *Radio Science*, *35*(4), 1025–1034, 2000.

Hinson, D. P., F. M. Flasar, A. J. K. P. J. Schinder, J. D. Twicken, and R. G. Herrera, Jupiter's ionosphere: Results from the first Galileo radio occultation experiment, *Geophysical Research Letters*, *24*(17), 2107–2110, 1997.

Hinson, D. P., J. D. Twicken, and E. T. Karayel, Jupiter's ionosphere: New results from the first Voyager 2 radio occultation measurements, *Jouranal of Geophysical Research*, *103*(A5), 2107–2110, 1998.

Hocke, K., A. G. Pavelyev, O. I. Yakovlev, L. Barthes, and N. Jakowski, Radio occultation data analysis by the radioholographic method, *Journal of Atmospheric and Solar-Terrestrial Physics*, *61*(15), 1169–1177, 1999.

Karayel, T. E., and D. P. Hinson, Sub-Fresnel scale resolution in atmospheric profiles from radio occultation, *Radio Science*, *32*(2), 411–423, 1997.

Korn, G., and T. M. Korn, *Mathematical Handbook*, McGraw-Hill, New York, 1968.

Kravtsov, Y. A., and Y. I. Orlov, *Geometrical optics of inhomogeneous media*, Springer, Berlin, 1990.

Kursinski, E. R., G. A. Hajj, J. T. S. R. P. Linfield, and K. R. Hardy, Observing Earth's atmosphere with radio occultation measurements using the Global Positioning System, *Journal of Geophysical Research*, *102*(D19), 23429–23465, 1997.

Lindal, G. F., J. R. Lyons, D. N. Sweetnam, V. R. Eshleman, and D. P. H. and. G. L. Tyler, The atmosphere of Uranus: Results of radio occultation measurements with Voyager 2, *Journal of Geophysical Research*, *92*(A13), 14987–15001, 1987.

Marouf, E. A., G. L. Tyler, and P. A. Rosen, Profiling Saturn rings by radio occultation, *ICARUS*, *68*, 120–166, 1986.

Martin, J., Simulation of wave propagation in random media: theory and applications, in *Wave propagation in random media (scintillations)*, edited by V. I. Tatarskii, A. Ishimaru, and V. U. Zavorotny, SPIE - The International Society for Optical Engineering and Institute of Physics Publishing, Bellingham, Washington USA, Bristol and Philadelphia, 1992.

Mishchenko, A. S., V. E. Shatalov, and B. Y. Sternin, *Lagrangian manifolds and the Maslov operator*, Springer-Verlag, Berlin - New York, 1990.

Pavel'ev, A. G., On possibility of radioholographic investigation of radiofields near radioshadow zone at radiocommunication link satellite-to-satellite, *Radiotekh. Elektron.*, *43*(8), 1998.

Phinney, R. A., and D. L. Anderson, On the radio occultation method for studying planetary atmospheres, *Journal of Geophysical Research*, *73*(5), 1819–1827, 1968.

Rocken, C., et al., Verification of GPS/MET data in the neutral atmosphere, *Journal of Geophysical Research*, *102*(D25), 29849–29866, 1997.

Santalo, L. A., *Integral geometry and geometric probability*, Addison-Wesley Pub. Co., Reading, Mass., 1976, xvii, 404 p. ill.

Steiner, A. K., G. Kirchengast, and H. P. Ladreiter, Inversion, error analysis, and validation of GPS/MET data, 1999.

Vladimirov, V. S., *Equations of mathematical physics*, Pure and applied mathematics, 3, M. Dekker, New York, 1971, vi, 418 p. illus. 24 cm.

Vorob'ev, V. V., and T. G. Krasil'nikova, Estimation of the accuracy of the atmospheric refractive index recovery from Doppler shift measurements at frequencies used in the NAVSTAR system, *Izvestiya Academy of Sciences SSSR, Atmospheric and Oceanic Physics, English Translation*, *29*(5), 602–609, 1994.

Ware, R., et al., GPS sounding of the atmosphere from Low Earth Orbit: Preliminary results, *Bulletin of the American Meteorological Society*, *77*(1), 19–40, 1996.

Zverev, V. A., *Radio-optics*, Soviet Radio, Moscow, 1975.

DANISH METEOROLOGICAL INSTITUTE

Scientific Reports

Scientific reports from the Danish Meteorological Institute cover a variety of geophysical fields, i.e. meteorology (including climatology), oceanography, subjects on air and sea pollution, geomagnetism, solar-terrestrial physics, and physics of the middle and upper atmosphere.

Reports in the series within the last five years:

No. 96-1
Poul Frich (co-ordinator), H. Alexandersson, J. Ashcroft, B. Dahlström, G.R. Demarée, A. Drebs, A.F.V. van Engelen, E.J. Førland, I. Hanssen-Bauer, R. Heino, T. Jónsson, K. Jonasson, L. Keegan, P.Ø. Nordli, **T. Schmith**, **P. Steffensen**, H. Tuomenvirta, O.E. Tveito: North Atlantic Climatological Dataset (NACD Version 1) - Final report

No. 96-2
Georg Kjærgaard Andreasen: Daily response of high-latitude current systems to solar wind variations: application of robust multiple regression. Methods on Godhavn magnetometer data

No. 96-3
Jacob Woge Nielsen, Karsten Bolding Kristensen, Lonny Hansen: Extreme sea level highs: a statistical tide gauge data study

No. 96-4
Jens Hesselbjerg Christensen, Ole Bøssing Christensen, Philippe Lopez, Erik van Meijgaard, Michael Botzet: The HIRLAM4 Regional Atmospheric Climate Model

No. 96-5
Xiang-Yu Huang: Horizontal diffusion and filtering in a mesoscale numerical weather prediction model

No. 96-6
Henrik Svensmark and Eigil Friis-Christensen: Variation of cosmic ray flux and global cloud coverage - a missing link in solar-climate relationships

No. 96-7
Jens Havskov Sørensen and Christian Ødum Jensen: A computer system for the management of epidemiological data and prediction of risk and economic consequences during outbreaks of foot-and-mouth disease. CEC AIR Programme. Contract No. AIR3 - CT92-0652

No. 96-8
Jens Havskov Sørensen: Quasi-automatic of input for LINCOM and RIMPUFF, and output conversion. CEC AIR Programme. Contract No. AIR3 - CT92-0652

No. 96-9
Rashpal S. Gill and Hans H. Valeur:
Evaluation of the radarsat imagery for the operational mapping of sea ice around Greenland

No. 96-10
Jens Hesselbjerg Christensen, Bennert Machenhauer, Richard G. Jones, Christoph Schär, Paolo Michele Ruti, Manuel Castro and Guido Visconti:
Validation of present-day regional climate simulations over Europe: LAM simulations with observed boundary conditions

No. 96-11
Niels Larsen, Bjørn Knudsen, Paul Eriksen, Ib Steen Mikkelsen, Signe Bech Andersen and Torben Stockflet Jørgensen: European Stratospheric Monitoring Stations in the Artic: An European contribution to the Network for Detection of Stratospheric Change (NDSC): CEC Environment Programme Contract EV5V-CT93-0333: DMI contribution to the final report

No. 96-12
Niels Larsen: Effects of heterogeneous chemistry on the composition of the stratosphere: CEC Environment Programme Contract EV5V-CT93-0349: DMI contribution to the final report

No. 97-1
E. Friis Christensen og C. Skøtt: Contributions from the International Science Team. The Ørsted Mission - a pre-launch compendium

No. 97-2
Alix Rasmussen, Sissi Kiilsholm, Jens Havskov Sørensen, Ib Steen Mikkelsen: Analysis of tropospheric ozone measurements in Greenland: Contract No. EV5V-CT93-0318 (DG 12 DTEE): DMI's contribution to CEC Final Report Arctic Trophospheric Ozone Chemistry ARCTOC

No. 97-3
Peter Thejll: A search for effects of external events on terrestrial atmospheric pressure: cosmic rays

No. 97-4
Peter Thejll: A search for effects of external events on terrestrial atmospheric pressure: sector boundary crossings

No. 97-5
Knud Lassen: Twentieth century retreat of sea-ice in the Greenland Sea

No. 98-1
Niels Woetman Nielsen, Bjarne Amstrup, Jess U. Jørgensen:
HIRLAM 2.5 parallel tests at DMI: sensitivity to type of schemes for turbulence, moist processes and advection

No. 98-2
Per Høeg, Georg Bergeton Larsen, Hans-Henrik Benzon, Stig Syndergaard, Mette Dahl Mortensen: The GPSOS project
Algorithm functional design and analysis of ionosphere, stratosphere and troposphere observations

No. 98-3
Mette Dahl Mortensen, Per Høeg:
Satellite atmosphere profiling retrieval in a nonlinear troposphere
Previously entitled: Limitations induced by Multipath

No. 98-4
Mette Dahl Mortensen, Per Høeg:
Resolution properties in atmospheric profiling with GPS

No. 98-5
R.S. Gill and M. K. Rosengren
Evaluation of the Radarsat imagery for the operational mapping of sea ice around Greenland in 1997

No. 98-6
R.S. Gill, H.H. Valeur, P. Nielsen and K.Q. Hansen: Using ERS SAR images in the operational mapping of sea ice in the Greenland waters: final report for ESA-ESRIN's: pilot projekt no. PP2.PP2.DK2 and 2nd announcement of opportunity for the exploitation of ERS data projekt No. AO2..DK 102

No. 98-7
Per Høeg et al.: GPS Atmosphere profiling methods and error assessments

No. 98-8
H. Svensmark, N. Woetmann Nielsen and A.M. Sempreviva: Large scale soft and hard turbulent states of the atmosphere

No. 98-9
Philippe Lopez, Eigil Kaas and Annette Guldberg: The full particle-in-cell advection scheme in spherical geometry

No. 98-10
H. Svensmark: Influence of cosmic rays on earth's climate

No. 98-11
Peter Thejll and Henrik Svensmark: Notes on the method of normalized multivariate regression

No. 98-12
K. Lassen: Extent of sea ice in the Greenland Sea 1877-1997: an extension of DMI Scientific Report 97-5

No. 98-13
Niels Larsen, Alberto Adriani and Guido Di-Donfrancesco: Microphysical analysis of polar stratospheric clouds observed by lidar at McMurdo, Antarctica

No.98-14
Mette Dahl Mortensen: The back-propagation method for inversion of radio occultation data

No. 98-15
Xiang-Yu Huang: Variational analysis using spatial filters

No. 99-1
Henrik Feddersen: Project on prediction of climate variations on seasonel to interannual timescales (PROVOST) EU contract ENVA4-CT95-0109: DMI contribution to the final report:Statistical analysis and post-processing of uncoupled PROVOST simulations

No. 99-2
Wilhelm May: A time-slice experiment with the ECHAM4 A-GCM at high resolution: the experimental design and the assessment of climate change as compared to a greenhouse gas experiment with ECHAM4/OPYC at low resolution

No. 99-3
Niels Larsen et al.: European stratospheric monitoring stations in the Artic II: CEC Environment and Climate Programme Contract ENV4-CT95-0136. DMI Contributions to the project

No. 99-4
Alexander Baklanov: Parameterisation of the deposition processes and radioactive decay: a review and some preliminary results with the DERMA model

No. 99-5
Mette Dahl Mortensen: Non-linear high resolution inversion of radio occultation data

No. 99-6
Stig Syndergaard: Retrieval analysis and methodologies in atmospheric limb sounding using the GNSS radio occultation technique

No. 99-7
Jun She, Jacob Woge Nielsen: Operational wave forecasts over the Baltic and North Sea

No. 99-8
Henrik Feddersen: Monthly temperature forecasts for Denmark - statistical or dynamical?

No. 99-9
P. Thejll, K. Lassen: Solar forcing of the Northern hemisphere air temperature: new data

No. 99-10
Torben Stockflet Jørgensen, Aksel Walløe Hansen: Comment on "Variation of cosmic ray flux and global coverage - a missing link in solar-climate relationships" by Henrik Svensmark and Eigil Friis-Christensen

No. 99-11
Mette Dahl Meincke: Inversion methods for atmospheric profiling with GPS occultations

No. 99-12
Benzon, Hans-Henrik; Olsen, Laust: Simulations of current density measurements with a Faraday Current Meter and a magnetometer

No. 00-01
Høeg, P.; Leppelmeier, G: ACE: Atmosphere Climate Experiment: proposers of the mission

No. 00-02
Høeg, P.: FACE-IT: Field-Aligned Current Experiment in the Ionosphere and Thermosphere

No. 00-03
Allan Gross: Surface ozone and tropospheric chemistry with applications to regional air quality modeling. PhD thesis

No. 00-04
Henrik Vedel: Conversion of WGS84 geometric heights to NWP model HIRLAM geopotential heights

No. 00-05
Jérôme Chenevez: Advection experiments with DMI-Hirlam-Tracer

No. 00-06
Niels Larsen: Polar stratospheric clouds microphysical and optical models

No. 00-07
Alix Rasmussen: "Uncertainty of meteorological parameters from DMI-HIRLAM"

No. 00-08
A.L. Morozova: Solar activity and Earth's weather. Effect of the forced atmospheric transparency changes on the troposphere temperature profile studied with atmospheric models

No. 00-09
Niels Larsen, Bjørn M. Knudsen, Michael Gauss, Giovanni Pitari: Effects from high-speed civil traffic aircraft emissions on polar stratospheric clouds

No. 00-10
Søren Andersen: Evaluation of SSM/I sea ice algorithms for use in the SAF on ocean and sea ice, July 2000

No. 00-11
Claus Petersen, Niels Woetmann Nielsen: Diagnosis of visibility in DMI-HIRLAM

No. 00-12
Erik Buch: A monograph on the physical oceanography of the Greenland waters

No. 00-13
M. Steffensen: Stability indices as indicators of lightning and thunder

No. 00-14
Bjarne Amstrup, Kristian S. Mogensen, Xiang-Yu Huang: Use of GPS observations in an optimum interpolation based data assimilation system

No. 00-15
Mads Hvid Nielsen: Dynamisk beskrivelse og hydrografisk klassifikation af den jyske kyststrøm

No. 00-16
Kristian S. Mogensen, Jess U. Jørgensen, Bjarne Amstrup, Xiaohua Yang and Xiang-Yu Huang: Towards an operational implementation of HIRLAM 3D-VAR at DMI

No. 00-17
Sattler, Kai; Huang, Xiang-Yu: Structure function characteristics for 2 meter temperature and relative humidity in different horizontal resolutions

No. 00-18
Niels Larsen, Ib Steen Mikkelsen, Bjørn M. Knudsen m.fl.: In-situ analysis of aerosols and gases in the polar stratosphere. A contribution to THESEO. Environment and climate research programme. Contract no. ENV4-CT97-0523. Final report

No. 00-19
Amstrup, Bjarne: EUCOS observing system experiments with the DMI HIRLAM optimum interpolation analysis and forecasting system

No. 01-01
V.O. Papitashvili, L.I. Gromova, V.A. Popov, O. Rasmussen, S. Vennerstrøm: Northern polar cap magnetic activity index PCN: Effective area, universal time, seasonal, and solar cycle variations
(In Press)